ADRANOS: a Numerical Tool to Define Suitable Operating Conditions for the EU-DEMO Divertor Cooling Circuit

A. Quartararo[a,*], P.A. Di Maio[a], E. Vallone[a]

[a]*Department of Engineering, University of Palermo, Viale delle Scienze, Ed. 6, 90128 Palermo, Italy*

Abstract

In the context of the activities of the EUROfusion action, the University of Palermo (UNIPA) has carried out a research campaign to evaluate the thermal-hydraulic performance of the DEMO divertor Single-Circuit Cooling (SCC) option. This cooling layout foresees the adoption of a single cooling circuit for the entire cassette and differs from the baseline DEMO divertor configuration where two separate and independent cooling circuits are employed for the Plasma Facing Components and the Cassette Body.

Given the exceptional geometric complexity of the component, the search for coolant operating conditions that comply with the applicable design constraints and requirements is very challenging and cannot be performed by relying on detailed 3D computational fluid dynamic calculations, due to the high computational cost that it would demand. For this purpose, the UNIPA thermo-hydraulic research unit has developed the Advanced Divertor paRametric Analysis for coolaNt Operating Scenarios (ADRANOS) code, a novel numerical tool able to quickly assess the thermofluid-dynamic behaviour of the divertor cooling circuit with a reduced computational effort, predicting the divertor performance map at different coolant inlet conditions and mass flow rates, and considering different circuit topologies.

ADRANOS is able to assess the mass flow rate, coolant temperature, and coolant pressure distribution among the different sub-components constituting the divertor cassette, by adopting a lumped-parameters approach. Moreover, a 2D-FEM module is embedded in the code allowing to evaluate the detailed temperature distribution inside the Plasma-Facing Unit structures, so to check the compliance with materials temperature limits under different thermal load conditions.

This work presents the code modelling approach, its validation and the application to the divertor SCC option in order to compare its thermal-hydraulic performance with the baseline divertor option, providing a basis for assessing the feasibility of this concept.

Keywords: DEMO, Divertor, Plasma facing components, Thermofluid-dynamics, Monoblock

1. Introduction

One of the main challenges in the realisation of a fusion reactor able to deliver electricity to the grid, such as the EU-DEMO, is the control of power exhaust, as emphasised by Mission 2 of the European Research Roadmap to the Realisation of Fusion Energy [1].

The divertor is a critical in-vessel component in this context and, apart from continuously removing the power deposited by charged particle bombardment and neutron irradiation, it has to cope with several other fundamental functions, such as ensuring the existence of channels through which to dispose of the ashes produced by fusion reactions, providing plasma-facing surfaces physically compatible with the plasma, and shielding the vacuum vessel and magnets from nuclear loads [2]. On the other hand, the component must also be designed to perform its functions according to certain fundamental engineering requirements, i.e. to reduce nuclear waste, to minimise costs and maximise the material recycling potential, and finally to minimise design complexity, aiming to reduce maintenance downtime, without impacting negatively the plant availability [3].

According to its baseline design [4], the EU-DEMO divertor consists of 48 toroidally-arranged cassette

*Corresponding author
Email address: andrea.quartararo@unipa.it (A. Quartararo)

modules. Each cassette, as depicted in fig. 1, comprises several sub-components: two Plasma-Facing Components (PFCs), also referred to as Vertical Targets (VTs), a Shielding Liner (SL), two Reflector Plates (RPs) and a Cassette Body (CB) supporting all the other sub-components.

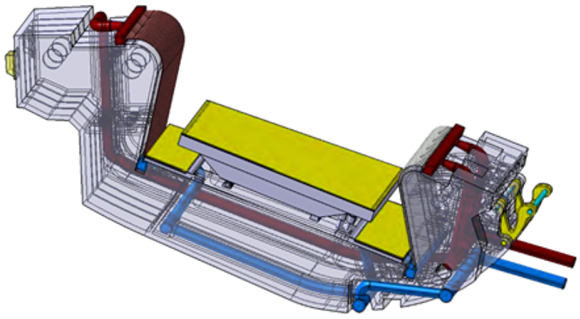

Figure 1: EU-DEMO divertor cassette (DCC option).

The EU-DEMO divertor baseline is based on the Double-Circuit Cooling (DCC) option concept, as it foresees two cooling circuits [2], one for the PFCs and one for the CB and the remaining sub-components, this latter simply referred to as CB cooling circuit. Sub-cooled pressurized water is employed as a coolant for both the cooling circuits, and, due to the specific thermal requirements of the different parts of the divertor, different coolant operating conditions are adopted. Therefore, two independent Primary Heat Transfer Systems (PHTSs) are foreseen in the baseline DEMO divertor design.

Although the Gate Review carried out at the end of the EU-DEMO Pre-Concept Design phase [5] endorsed the divertor baseline design and the selected technologies adopted, it was also suggested to investigate the possibility of employing a Single-Circuit Cooling (SCC) option cassette, aiming to allow for a simpler balance of plant design, as this solution would require a single PHTS, and to ease remote maintenance, since only one inlet and one outlet pipe should be cut and reweld for each cassette during replacement operations.

In the context of the EUROfusion action, the University of Palermo (UNIPA) thermal-hydraulic research team has developed a calculation tool dedicated to studying the thermofluid-dynamic behaviour of the divertor cooling circuit. This novel tool, named Advanced Divertor paRametric Analysis for coolaNt Operating Scenarios (ADRANOS), has been conceived to predict, with a reduced computational effort, the divertor thermal-hydraulic performance map with the aim of evaluating suitable coolant operating conditions to be adopted for the SCC divertor cooling circuit, providing a basis for assessing the feasibility of this concept.

2. The DEMO divertor cooling circuits

The divertor cooling circuits are designed to allow removing the surface and volumetric heat loads expected during normal and off-normal operation, ensuring that structural and functional materials work within their optimal temperature ranges, so as to safely achieve the divertor desired target functions and requirements throughout its envisaged lifetime.

The nominal surface heat loads relevant to the EU-DEMO divertor are reported in table 1, while maximum volumetric heat loads around 12 MW/m^3 [6] are expected for the cassettes. With reference to the table, the slow transient events are either normal or off-normal transient plasma scenarios whose duration is in the order of 10s of seconds [2].

Table 1: Nominal heat fluxes prescribed for the EU-DEMO divertor [2].

Heat Fluxes	**Value**
Maximum heat flux on VTs during normal operation	≈10 MW/m^2
Maximum heat flux on VTs during slow transient events	≈20 MW/m^2
Maximum heat flux on SL during normal operation	≈1 MW/m^2
Maximum heat flux on RPs during normal operation	≈0.2 MW/m^2

As it may be argued from the table, there is an order of magnitude of difference between the surface loads foreseen on the VTs and those of the other divertor sub-components. This difference is the motivation for the selection of separate cooling circuits for the baseline EU-DEMO divertor, as will be detailed in the following section.

2.1. Divertor double-circuit cooling option

As described in [7], the PFCs cooling circuit has been conceived to withstand the exceptional heat fluxes reported in table 1, which are concentrated within a narrow band (the poloidal extension of the region where these values are expected is approximately ±50 mm around the strike point [2]), resulting in a peaked power distribution. The PFCs cooling thus requires high mass flow rates of low-temperature water, resulting in average velocities inside the cooling channels in the range of 12 - 15 m/s [8], so to guarantee a sufficient safety margin

against the Critical Heat Flux (CHF) occurrence, in order to avoid dry-out phenomena that could jeopardize the target structural integrity.

The DCC PFCs cooling circuit foresees the two VTs connected in parallel. These are composed of a toroidal array of 31 and 43 Plasma Facing Unit (PFU) assemblies, respectively for the Inner VT (IVT) and the Outer VT (OVT) [9].

The pipes and distributors/manifolds composing the PFCs cooling circuit are made of AISI 316 [10], while each PFU assembly consists of a long cooling pipe made of CuCrZr equipped with a Swirl Tape (ST) turbulence promoter, covered with a longitudinal array of tungsten tiles, namely monoblocks, joined to the CuCrZr pipe by means of a thin copper interlayer. An exploded view of a divertor PFU assembly foreseen for the EU-DEMO divertor is depicted in fig. 2.

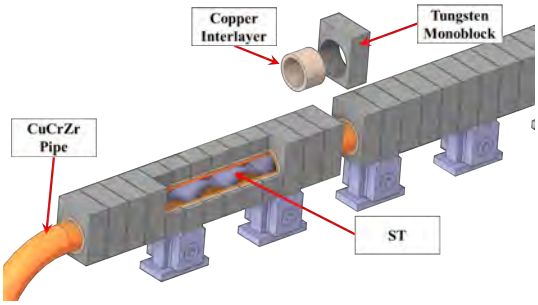

Figure 2: Exploded view of a divertor PFU assembly.

The DCC PFCs cooling circuit is depicted in fig. 3, while its schematic flowchart is shown in fig. 4, with the indications of temperatures, pressures, and mass flow rates, according to the results reported in [8].

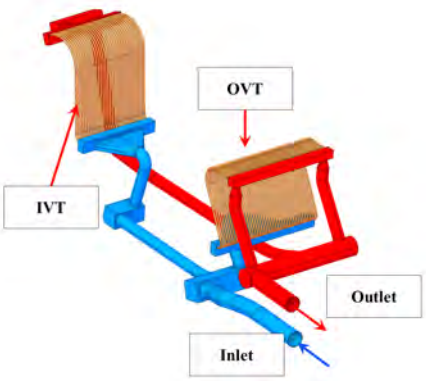

Figure 3: EU-DEMO divertor PFCs cooling circuit (DCC option, 2019 design).

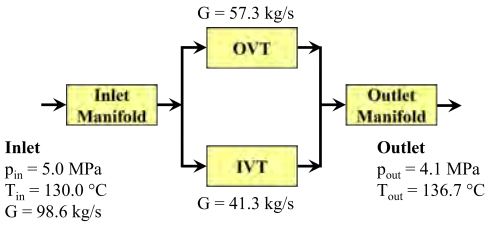

Figure 4: EU-DEMO divertor PFCs cooling circuit scheme (DCC option, 2019 design).

The DCC option CB cooling circuit is meant to provide cooling to the CB, SL, and RPs. These components are made of Eurofer and both SL and RPs are equipped with a thin tungsten layer in the surfaces directly exposed to the plasma. The cooling circuit layout is shown in fig. 5, while its cooling scheme is visible, with temperature, pressure and flow rate indications, in fig. 6, according to the results reported in [11].

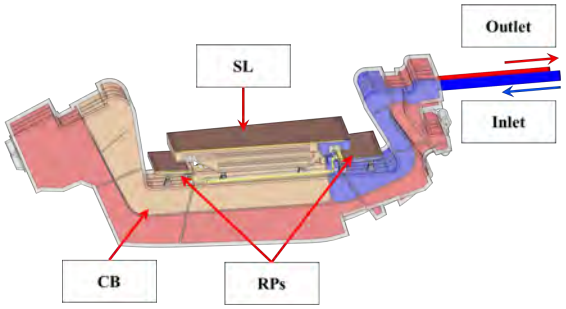

Figure 5: EU-DEMO divertor CB cooling circuit (DCC option, 2019 design).

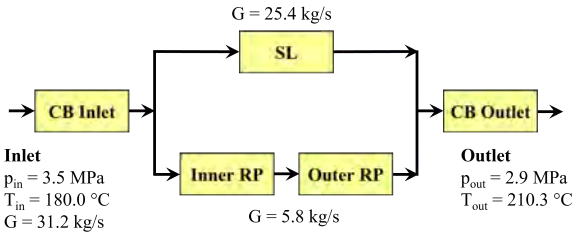

Figure 6: EU-DEMO divertor CB cooling circuit scheme (DCC option, 2019 design).

As can be noted from fig. 6, the CB cooling circuit is supplied with cooling water at a higher temperature compared to the PFCs, while both mass flow rate and pressure are lower. These coolant operating conditions are allowed by the significantly lower thermal loads ex-

pected for the CB, SL, and RPs (table 1), and are necessary to adopt Eurofer as structural material, requiring higher operating temperatures to comply with resilience requirements for the expected lifetime.

2.2. *Divertor single-circuit cooling option*

As an alternative to the baseline design, the SCC option divertor cassette developed for EU-DEMO in 2021 [12] is depicted in fig. 7. As can be seen from the figure and similarly to the DCC option, the cassette is made of Eurofer and is equipped with two VTs, one SL, two RPs, and additionally a pair of Neutron Shields (NSs) to improve neutron shielding in the vacuum pumping hole. It appears clear that the complexity of the SCC divertor cooling circuit is much greater than that of the DCC, as confirmed by the cooling scheme shown in fig. 8.

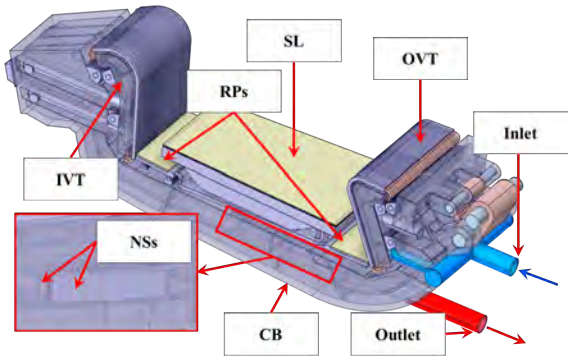

Figure 7: EU-DEMO divertor cassette (SCC option, 2021 design).

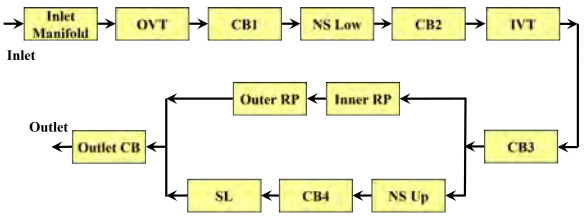

Figure 8: EU-DEMO divertor cooling circuit scheme (SCC option, 2021 design).

The coolant mass flow rate and inlet operating conditions to be adopted for the EU-DEMO divertor SCC option must comply with the requirements of both the VTs and the Eurofer sub-components of the cassette, and are yet to be selected.

A 3D Computational Fluid-Dynamic (CFD) simulation of the SCC divertor has been performed in [6], tentatively considering cooling water at 130°C and 70 bar and with the highest coolant mass flow rate allowed to stay within the maximum pressure drop limits. Under these operating conditions, insufficient CHF margins for the VTs have been observed.

However, different coolant operating conditions or cooling circuit layouts of the SCC option could be able to guarantee the compliance with several design constraints and requirements for the divertor, which are detailed in the following section.

3. Thermal and thermo-hydraulic constraints

The design of the EU-DEMO divertor cooling circuits has been driven by the following set of design constraints, drawn from [9], which are only relevant to purely thermal-hydraulic aspects.

1. Maximum water axial velocity in PFU cooling channels lower than 16 m/s;
2. water total pressure drop for each cooling circuit lower than 14 bar;
3. CHF margin of VTs higher than 1.4 under the nominal heat flux of 20 MW/m^2;
4. CHF margin of SL and RPs higher than 1.4 under the nominal heat fluxes of respectively 1 and 0.2 MW/m^2;
5. minimum margin against saturation temperature higher than 20°C.

For the case of the DCC option, the PFCs cooling circuit had to comply with constraints 1 to 3, while the CB cooling circuit to 2, 4, and 5. The SCC option, instead, has to be designed to meet all these constraints, while the maximum pressure drop of 14 bar is inclusive of the CB, SL,RPs, NSs, and VTs contributions. The compliance with the constraints listed above can be verified based on rather simple calculations by applying the First Principle of Thermodynamics and adopting appropriate correlations, for example following the procedure described in [13].

Additionally, the cooling circuit should allow structural and functional materials to operate inside prescribed temperature ranges in normal and off-normal operating conditions, either stationary or transient, to ensure a suitable thermo-structural performance and an adequate lifetime of the components. Given the geometrical complexity of the divertor, an accurate estimation of the temperature distribution in structures must rely on the adoption of complex 3D coupled (fluid-structure) thermofluid-dynamics calculations. However, it is possible to assess with good confidence and with simple steady-state 2D calculations the maximum temperatures reached within the most critical components

from a thermal standpoint, i.e. the PFUs. It is feasible due to their relatively simple geometry together with the peaked shape of the surface power density and the low thermal inertia of these components, which reach stationary conditions within a few tens of seconds, as can be argued from [14].

In this work, the following set of constraints on the acceptable temperatures relevant to the PFU materials is considered, in accordance with [15]:

- maximum tungsten temperature lower than 3222°C (200°C margin against melting);
- maximum copper interlayer temperature lower than 885°C (200°C margin against melting);
- maximum allowable CuCrZr pipe temperature below 300°C at 10 MW/m^2 (to be calculated as average over the pipe thickness) to guarantee negligible creep;
- maximum allowable CuCrZr pipe temperature below 450°C at 20 MW/m^2 (to be calculated as average over the pipe thickness) to guarantee negligible creep.

This list of temperature constraints is not meant to be exhaustive but can be verified very easily and allows for an initial screening of unsuitable divertor coolant operating conditions.

Additionally, reference will be made in this work to the allowable temperature of Eurofer. Although the optimal operating temperature range for this material is 350-550°C [2], the design of the divertor cassette has been carried out over the last years considering a Eurofer minimum operating temperature of 180°C, according to the rationale described in [16]. Operating the divertor at these low temperatures implies a strong constraint on the maximum irradiation damage dose, finally resulting in a component lifetime that, for the case of the baseline cassette SL, is expected to be 1.2 Full Power Year (fpy), currently lower than the target lifetime of 1.5 fpy [2]. It is also easy to see how, according to what is reported in [16], every increase in the CB coolant temperature would lead to an increase in the lifetime of the component and, vice versa, every reduction in coolant temperature would lead to a reduction of the lifetime. It should be moreover taken into account that a relaxed conservativism of the mechanical design rules may allow for an increase in the divertor lifetime [2] with respect to the values actually considered, and therefore, the results presented here may be conservative.

With simple numerical tools, it is not possible to check the compliance with the upper limit of the Eurofer temperature range but, nevertheless, the component lifetime can be easily estimated, as the lower temperature of the structure will surely be the inlet temperature of its cooling water.

4. ADRANOS development

4.1. Overview

ADRANOS is a coupled lumped-parameter/2D Finite Element Method (FEM) simulation tool created with the aim of assessing the steady-state performance map of the DEMO divertor cooling circuit, to be intended as the domain of the phase space of coolant inlet mass flow rate, pressure and temperature conditions that allow the cooling system to safely carry out its target mission. In particular, it allows parametric analyses to be performed over a great number of different configurations and inlet coolant conditions with an acceptable computational effort, evaluating the compliance with the set of constraints discussed in the previous paragraph. The code has been developed in MATLAB [17] with an object-oriented approach, to make it highly flexible in evaluating different cooling system topologies, and it has been optimized for parallel computing, so to greatly reduce the overall time required to perform the simulations.

The code takes advantage of the FEA toolbox [18] FEM solver available in the MATLAB package, with the aim to perform 2D steady-state thermal analyses of the PFU monoblocks located at the IVT and OVT strike points, thus evaluating the temperature distribution in the most critical region of the PFCs.

The methodologies and procedures implemented in ADRANOS are based on the work of [19, 20, 21, 22]. The element of novelty introduced with respect to other codes is the coupling between the lumped-parameter simulation of the entire EU-DEMO divertor cooling circuit and the FEM module, as well as the adoption of this methodology as a screening tool capable of delimiting the range of suitable coolant operating conditions to be employed for a given divertor cooling circuit layout.

4.2. Methodology - Lumped parameters module

ADRANOS evaluates the steady-state temperature and pressure distribution within the considered cooling circuit, by adopting a theoretical approach based on the lumped-parameter method. The layout of the input cooling circuit is provided to the code in the form of a flowchart, similar to those reported in figs. 4, 6 and 8. The cooling circuit must be at first subdivided into different volumes, each one representing a relevant subcomponent to be analysed in detail. The volumes can be

connected in series or parallel, and it is furthermore possible to group them so to ease the circuit definition, as well as to perform more detailed 1D assessments (e.g. if it is required to obtain pressure and/or temperature profiles).

The code relies on preliminary thermofluid-dynamic analyses performed with dedicated 3D-CFD calculations, whenever the geometric complexity of the volumes in which the cooling circuit is subdivided is too great to allow characteristic curves to be defined on the basis of simple correlations. Therefore, each volume entails being provided with the hydraulic characteristic equation $\Delta p(G)$, defined according to eq. (1), where Δp is the total pressure drop, ρ is the average density calculated starting from the average values of temperature $\overline{T}$ and pressure $\overline{p}$ inside the volume (arithmetic averages between inlet and outlet conditions), and G is the mass flow rate.

$$\Delta p = \frac{\rho_{ref}}{\rho\left(\overline{T}, \overline{p}\right)} \alpha G^{\gamma} \tag{1}$$

More in detail, starting from the results of CFD simulations, i.e. a set of Δp values at different mass flow rates, a curve with the general form $\Delta p = \alpha \dot{G}^{\gamma}$ is fitted, where α and γ are proper fitting coefficients. To take then into account the variation of pressure drop with the coolant temperature, the density correction $\rho_{ref}/\rho\left(\overline{T}, \overline{p}\right)$ is considered, following the rationale reported in [13], where the reference density ρ_{ref} is calculated from the supporting CFD simulations a proper volume-averaged density value.

The code solves sequentially the cooling circuit, starting from the inlet volume and proceeding downstream to the outlet of the circuit. For each volume, for a given set of inlet conditions T_{in}, p_{in} and a given G, the energy conservation equation in steady-state conditions eq. (2) and pressure drop equation eq. (3) are solved iteratively. With reference to the following equations, c_p is the fluid heat capacity under isobaric conditions calculated at the volume average values of pressure and temperature and W is the total power (sum of surface and volumetric heat loads) deposited onto the volume.

It is worth mentioning that, as far as all the thermodynamic and transport properties of water are concerned, these are calculated by adopting a MATLAB implementation [23] of the IAPWS IF97 water library [24].

$$T_{out}^{i} = T_{in} + \frac{W}{G c_p\left(\overline{T}^{i-1}, \overline{p}^{i-1}\right)} \tag{2}$$

$$p_{out}^{i} = p_{in} - \frac{\rho_{ref}}{\rho\left(\overline{T}^{i-1}, \overline{p}^{i-1}\right)} \alpha G^{\gamma} \tag{3}$$

At each iteration i, outlet temperature and pressure values are updated adopting the fluid properties obtained from the previous iteration, and the calculation proceeds until relative errors of outlet temperature and pressures calculated at two consecutive iterations result lower than a given tolerance, set equal to 0.01%.

Special attention has to be paid when volumes are arranged in parallel. The code is currently able to handle only the parallel connection of two components (namely A and B). In particular, an additional outer loop is performed, adopting an optimization algorithm to find the value of the branching factor χ, defined according to eq. (4) (where G_A the mass flow rate flowing inside the branch A), such that the difference between the pressure drops in the two branches is the same.

$$\chi = \frac{G_A}{G} \tag{4}$$

The factor χ is iteratively updated by adopting the Golden-section search algorithm [25], until the ratio between the pressure drop unbalance between the branches and the average pressure drop reaches values below a given tolerance, chosen equal to 0.01%. Each optimization outer iteration requires an inner loop to obtain consistent values of pressure and temperature, according to eq. (2) and eq. (3).

Once the iterative procedure converges, the outlet pressure (the same for the two branches) is adopted as input value for the following volume, while the temperature to be passed downstream is obtained by solving the energy conservation law for two mixing flows of eq. (5), where h is the fluid specific enthalpy.

$$h_{out}\left(T_{out}, p_{out}\right) = \chi h_{out,A}\left(T_{out,A}, p_{out}\right) + \\ + (1-\chi)\, h_{out,B}\left(T_{out,B}, p_{out}\right) \tag{5}$$

When average temperature and pressure values are available for all the components, the lowest margin against saturation is assessed according to eq. (6), where T_{sat} is the saturation temperature calculated at the outlet volume pressure. This variable is estimated and stored for each volume, and the minimum value over the entire cooling circuit is successively compared with the applicable constraint.

$$\Delta T_{sat} = T_{sat}\left(p_{out}\right) - T_{out} \tag{6}$$

Special attention is moreover paid to the VT volumes, which require an additional estimation of the CHF margin and maximum coolant velocity. Each VT volume must be provided with the number and geometrical details of the PFU cooling channels, i.e. the CuCrZr tube diameter, the thickness and the twist ratio of the ST.

Firstly, the average coolant axial velocity along PFU cooling channels is determined according to eq. (7), where A is the cross-section of each channel while n is the number of PFU cooling channels of the selected VT.

$$\overline{v} = \frac{G}{nA\rho\left(\overline{T}, \overline{p}\right)} \tag{7}$$

Given the axial fluid velocity, the fluid average thermodynamic conditions and the geometrical details of the PFU cooling channels, the CHF margin can be derived according to the procedure described in [26], by adopting the well-known Tong-75 correlation of eq. (8) to calculate the CHF, where f is the Fanning friction factor, calculated according to eq. (9), r is the enthalpy of vaporization, p_{crit} is the water critical pressure (22.064 MPa), Re is the Reynolds number, calculated according to eq. (10), Ja is the Jacob number, calculated as per eq. (11), and finally C_f is a factor to account for the specific geometrical configuration, that, for the case of an ST-equipped tube can be assumed equal to 1.67.

$$CHF = 0.23 f \frac{G}{A} r C_f \cdot \cdot \left[1 + 0.00216\left(\frac{\overline{p}}{p_{crit}}\right)^{1.8} Re^{0.5} Ja\right] \tag{8}$$

$$f = 8Re^{-0.6}\left(\frac{d_h}{d_0}\right)^{0.32} \tag{9}$$

$$Re = \frac{\overline{v} d_h \rho\left(\overline{T}, \overline{p}\right)}{\mu_b\left(\overline{T}, \overline{p}\right)} \tag{10}$$

$$Ja = \frac{\rho\left(\overline{T}, \overline{p}\right)}{\rho_v} \cdot \frac{c_p\left(T_{sat} - \overline{T}\right)}{r} \tag{11}$$

With reference to equations eqs. (8) to (11), d_h is the PFU cooling channel hydraulic diameter that can be calculated with eq. (12), where d_i is the pipe inner diameter and δ is the ST thickness, d_0 is a reference diameter equal to 12.7 mm, μ_b is the water bulk dynamic viscosity, while ρ_v is the water vapour saturation density calculated at the fluid pressure. Moreover, the average block pressure $\overline{p}$ is calculated net of the fluid dynamic pressure $\frac{1}{2}\rho\left(\overline{T}, \overline{p}\right)\overline{v}^2$, and the calculation of the CHF is made assuming that at the strike point the coolant is at the average water thermodynamic conditions within the VT volume.

$$d_h = \frac{\pi d_i - 4\delta}{\pi + 2 - 2\delta/d_i} \tag{12}$$

Once the CHF is calculated, it is compared with the maximum heat flux $q_{w,max}$ expected at the interface between the PFU cooling channel and the coolant, obtained by multiplying the 20 MW/m^2 nominal heat flux onto the armour plasma-facing surface by a peaking factor (equal to 1.60 for the considered monoblock geometry) to take into account the uneven distribution of the heat flux around the pipe diameter. The CHF margin definition is given in eq. (13), where the factor 0.95 is required to take into account the uneven flow distribution among PFU cooling channels, supposing a 5% deviation from average CHF value, conservatively taken on the basis of the 3D-CFD calculation results of the entire EU-DEMO divertor PFCs cooling circuit.

$$M_{CHF} = 0.95\frac{CHF}{q_{w,max}} \tag{13}$$

Finally, concerning the maximum velocity in the PFU cooling channels, it is calculated for each VT by increasing the average velocity of eq. (7) of 5%, again in accordance with the results of the 3D-CFD simulations.

ADRANOS, once supplied with the range and the number of sample points to be considered for inlet pressure, inlet temperature and mass flow rate, performs all the calculations described above in order to assess, for each triplet (p_{in}, T_{in}, G), whether the cooling circuit is able to provide results compatible with the constraints of maximum pressure drop, minimum saturation margin, adequate CHF margin and maximum PFU channel coolant velocities for both IVT and OVT, in accordance with the limits listed in section 3. The CHF margin on SL and RPs is not currently calculated by the code, as it has been shown to be usually much higher than the prescribed constraint in [6, 11].

4.3. Methodology - 2D FEM thermal analyses module

The ADRANOS FEM module performs 2D steady-state thermal simulations of a section of the monoblock located at the strike point. The calculations are performed both for IVT and OVT and considering surface heat loads under normal operation and during slow transient conditions, considering the heat fluxes reported in table 1.

The geometrical details of the domain considered are depicted in fig. 9 while the mesh adopted for the 2D simulations is shown in fig. 10 (only half domain has been taken into account for symmetry), showing the different regions, characterized by different materials (tungsten, CuCrZr and copper), as well as the nomenclature adopted for the boundaries.

The computational mesh, whose details are summarized in table 2, has been selected by preliminary performing a grid-independence assessment considering both 10 and 20 MW/m^2 incident heat fluxes. The results of the analysis campaign, not reported here for the sake of brevity, showed how adopting the selected mesh, the errors with respect to the "grid-independent results" obtained by a generalized Richardson extrapolation procedure, as defined in [27], are well below 1% for maximum temperatures in tungsten, copper, and CuCrZr.

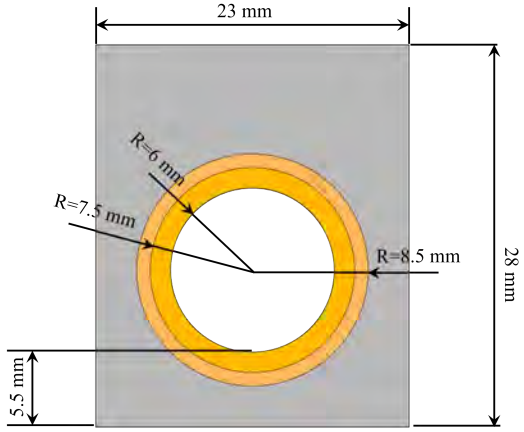

Figure 9: Geometrical details of the EU-DEMO PFU monoblock slice.

Table 2: Summary of the main mesh parameters.

Mesh Parameter	Value
Nodes	1279
Elements	2384
Elements Order and Topology	Linear Tria
Maximum Element Size [mm]	0.5
Minimum Element Size [mm]	0.25
Mesh Growth Rate	1.5

The 2D thermal steady-state simulations have been carried out considering the Boundary Conditions (BCs) given in table 3, while volumetric nuclear loads have been neglected. Concerning the materials, temperature-dependent properties have been considered for tungsten, CuCrZr and copper, respectively taken from [28], [29] and [30].

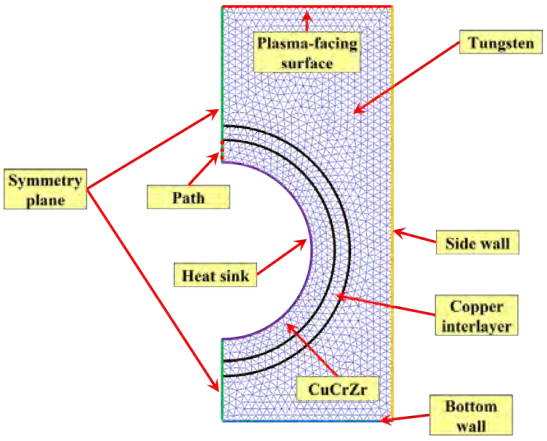

Figure 10: Mesh adopted for the monoblock steady-state thermal simulations with indications of the regions and boundary nomenclature.

Table 3: Summary of BCs adopted for the simulations.

Boundary	Applied BC
Plasma-facing wall	Heat flux of 10 and 20 MW/m^2
Bottom and side walls	Adiabatic
Symmetry plane	Symmetry
Heat sink	Robin BC

Regarding the heat sink, the Robin BC, necessary for the well-posedness of the problem and reported in table 3, is calculated depending on the local CuCrZr temperature, as well as on the pressure and temperature values of the coolant, by adopting the procedure described in the next section.

4.3.1. Heat Transfer Coefficient Calculation

In order to assess the temperature distribution in the PFUs, it is necessary to correctly reproduce the convective heat transfer mechanisms involved. This is only possible if a model capable of predicting the part of the Nukiyama boiling curve of interest is available. The selected correlations, calculated at each node of the heat sink boundary, are herewith reported.

Single-phase Forced Convection Heat Transfer

For the calculation of the single-phase convective heat transfer coefficient, ADRANOS adopts the Sieder-Tate correlation [31] (valid for $Re > 10000$ and a broad range of Prandtl number Pr) with the Gambill correction factor [32] to take into account the presence of the ST, as reported in eq. (14).

$$Nu = 0.027 Re^{0.8} Pr\left(\overline{T}, \overline{p}\right)^{1/3} \cdot \cdot \left(\frac{\mu_b\left(\overline{T}, \overline{p}\right)}{\mu_w\left(T_w, \overline{p}\right)}\right)^{0.14} \left(2.18 y^{-0.09}\right) \quad (14)$$

With reference to eq. (14), Nu is the Nusselt number, Pr is calculated at the coolant average pressure and temperature, μ_w is the water dynamic viscosity calculated at the average coolant pressure and considering the local wall temperature T_w, while y is the ST twist ratio. From eq. (14) is then possible to calculate the heat transfer coefficient and thus to evaluate the local heat flux q_{sp}, according to eq. (15), where λ is the bulk fluid heat conductivity.

$$q_{sp} = \frac{Nu\lambda\left(\overline{T}, \overline{p}\right)}{d_h}\left(T_w - \overline{T}\right) \quad (15)$$

This latter equation is required to calculate the heat transfer coefficient in two-phase heat transfer conditions.

Two-phase Forced Convection Heat Transfer

The correlations used for the various regimes of the Nukiyama boiling curve are taken entirely from the procedure described in [20] and [33].

Boiling incipience is evaluated by adopting the Bergles-Rohsenow onset of nucleate boiling correlation, reported in eq. (16), where the average pressure $\overline{p}$ is expressed in bar. The correlation is valid for water only, for a pressure range between 0.1 and 13.8 MPa [33].

$$q_{bi} = 1082\overline{p}^{1.156}\left(1.799\left(T_w - T_{sat}\right)\right)^{\frac{2.1598}{\overline{p}^{0.0234}}} \quad (16)$$

Fully developed nucleate boiling is evaluated with the Araki correlation, reported in eq. (17), while the partially developed nucleate boiling is calculated with the Bergles-Rohsenow correlation (eq. (18)).

$$q_{fdnb} = 10^6\left(\frac{T_w - T_{sat}}{\left(25.72 e^{\frac{-\overline{p}}{86}}\right)}\right)^3 \quad (17)$$

$$q_{pdnb} = \sqrt{q_{sp}^2 + \left(q_{fdnb} - q_{bi}\right)^2} \quad (18)$$

Although Araki's correlation is derived from experiments conducted with inlet pressures up to 13 bar and temperatures up to 80°C, in [33] it is adopted up to significantly higher values of the two parameters, maintaining a very good agreement with the experimental data.

More in detail, according to the rationale defined in [34], the two-phase flow regime is calculated by adopting the partially developed nucleate boiling of eq. (18). With this formulation, the heat flux asymptotically approaches fully developed boiling at high wall superheat. In particular, when the heat flux calculated with eq. (15) is lower than the one of eq. (16), the formulation given in eq. (15) is applied, otherwise, the heat flux is evaluated by adopting eq. (18).

Finally, as regards the calculation of the CHF and the estimation of the post-CHF heat transfer regime, it should be noted that, according to the constraints discussed in section 3, the divertor cooling circuit should allow operation with a CHF margin always higher than 1.4. Consequently, the post-CHF heat transfer coefficient calculation has not been currently implemented in ADRANOS, and the FEM module is executed uniquely when a CHF margin higher than 1 is obtained with the lumped-parameters module. When the CHF margin is lower than 1, instead, temperature values exceeding the pertaining limits are assigned on tungsten, copper, and CuCrZr.

Under both single-phase and two-phase heat transfer conditions, an equivalent convective heat transfer coefficient is calculated, simply by dividing the heat flux by the temperature difference between fluid bulk and wall, and assigned to the heat sink surface.

5. ADRANOS validation

To check the correctness of the implementation, the ADRANOS code has undergone a validation campaign of both the FEM and the lumped-parameters modules. First of all, the experimental setup of [35] has been reproduced, and the outcomes of the stand-alone FEM module have been compared to experimental data. Then, the divertor PFCs cooling circuit of the DCC option has been studied, to check if the ADRANOS outputs under design operating conditions are in agreement with the CFD calculation and if the temperature distributions in the monoblocks are in line with the results available in literature.

5.1. Marshall's experimental results validation case

The ADRANOS FEM module has been validated by comparing the code predictions with the experimental results obtained by Mashall [36] and reported in

[37]. The comparison has been performed by reproducing Marshall's experimental setup reported in [35], by looking at the temperature of the Oxygen-Free High-Conductivity (OFHC) copper monoblock at the thermocouple location, i.e. 0.6 mm from the plasma-facing surface on the side of the monoblock, as shown in fig. 11. The comparison between experimental and ADRANOS results is depicted in fig. 12.

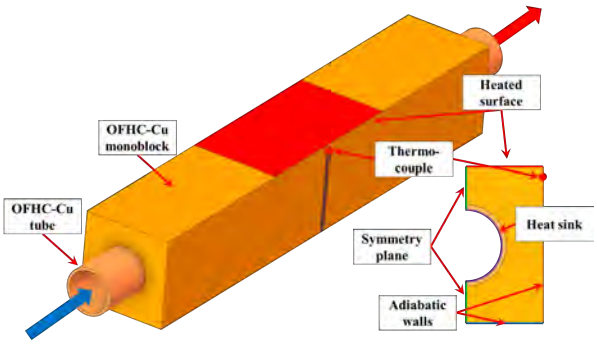

Figure 11: Experimental setup adopted by Marshall and detail of the ADRANOS 2D domain.

As can be seen, there is a very good correspondence between the ADRANOS results and the experimental data, with errors in predicting thermocouple temperatures within the ±10% range. At high heat flux values, a significant deviation between the curves is observed, related to the occurrence of the post-CHF heat transfer regime, not predicted by the calculation tool. Nevertheless, this does not impair the code predictive potential, since the divertor cooling circuit should operate far from this regime, as already discussed.

5.2. *DEMO divertor PFCs cooling circuit validation case*

The parametric study of the PFCs cooling circuit (DCC option, 2019 design) has been carried out starting from the layout shown in fig. 4.

The ADRANOS volumes have been defined considering integral surface and volumetric heat loads drawn from [9] while, concerning the characteristic curves, reference was made to the pressure drop breakdown reported in [8]. Since simulations of the PFCs cooling circuit at different mass flow rates are not available, a value of 2 was chosen for the γ exponent of eq. (1).

The analysis has been therefore carried out by keeping the coolant inlet pressure fixed at 50 bar while varying both the inlet temperature and the overall flow rate, respectively from 70 to 180°C and from 50 to 150 kg/s. The selected inlet temperature and mass flow rate ranges

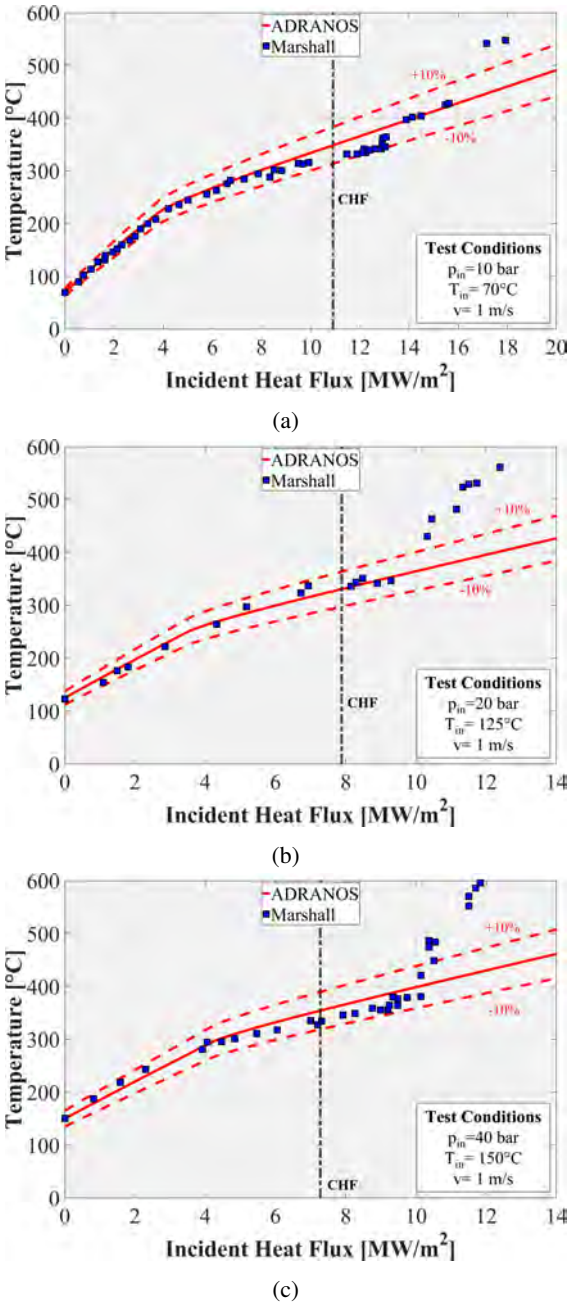

Figure 12: Comparison between ADRANOS and Marshall's experimental results at inlet pressure of 10 (a), 20 (b) and 40 (c) bar.

were discretized with 30 points each, for a total of 900 cases, while the overall run time to perform all the simulations was of approximately 13 minutes on a 3.00 GHz 18 core i9-9980XE workstation.

The results obtained are shown in fig. 13, with reference to the constraints listed in table 4. The figure also shows in red the PFCs cooling circuit design op-

erating point, i.e. G=98.58 kg/s and T_{in}=130°C, while the region in which the circuit can operate being compliant with all the selected constraints at the given inlet coolant pressure is filled in green.

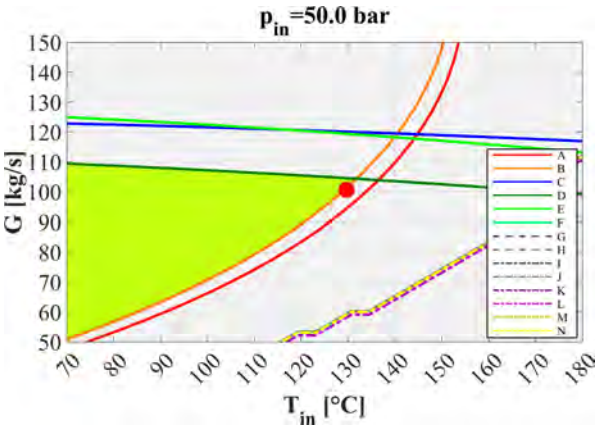

Figure 13: Range of acceptable operating conditions for the PFCs cooling circuit (DCC option, in green) and design operating point (in red).

Table 4: List of constraints and their IDs considered for the simulations.

ID	Constraint	Region	Load
A	$M_{CHF} = 1.4$	OVT	20 MW/m^2
B	$M_{CHF} = 1.4$	IVT	20 MW/m^2
C	$\Delta p = 14bar$	All	-
D	$v_{max} = 16m/s$	OVT	-
E	$v_{max} = 16m/s$	IVT	-
F	$\Delta T_{sat} = 20°C$	All	-
G	$T_{max} = 300°C$	OVT CuCrZr	10 MW/m^2
H	$T_{max} = 300°C$	IVT CuCrZr	10 MW/m^2
I	$T_{max} = 450°C$	OVT CuCrZr	20 MW/m^2
J	$T_{max} = 450°C$	IVT CuCrZr	20 MW/m^2
K	$T_{max} = 3222°C$	OVT tungsten	20 MW/m^2
L	$T_{max} = 3222°C$	IVT tungsten	20 MW/m^2
M	$T_{max} = 885°C$	OVT Cu	20 MW/m^2
N	$T_{max} = 885°C$	IVT Cu	20 MW/m^2

It should also be pointed out that, with regard to the maximum temperatures within the CuCrZr cooling pipe, these are calculated as average values along the path shown in fig. 10.

A comparison between the results obtained by ADRANOS for the design operating point with those of the 3D-CFD analysis of [8] is reported in table 5. As it may be argued from the table, there is a very good prediction of the overall pressure drop, of the flow distribution between the VTs, of the maximum fluid velocities that occur in the targets, and of the CHF margins, with relative errors below 3%. Furthermore, the results obtained with ADRANOS are conservative if compared to those of the detailed CFD calculations. These findings are not surprising since the ADRANOS simulations were set up on the basis of the results of the 3D-CFD analysis.

Table 5: Comparison between ADRANOS and CFD results.

	CFD	**ADRANOS**
Δp_{tot} [bar]	9.40	9.43
$\overline{v}_{OVT}$ [m/s]	14.91	15.09
$\overline{v}_{IVT}$ [m/s]	13.18	13.22
$M_{CHF,OVT}$ [-]	1.49	1.43
$M_{CHF,IVT}$ [-]	1.41	1.38

To further validate the ADRANOS FEM module, fig. 14 shows the thermal field predicted by the code for an OVT PFU considering the PFCs cooling circuit coolant under design conditions and under an incident heat flux of 10 MW/m^2 (similar results are obtained for the IVT). As can be observed, the maximum temperature predicted in tungsten is around 1100°C, in good agreement with the value reported in [2]. Considering instead an incident heat flux of 20 MW/m^2, the temperature distribution depicted in fig. 15 is obtained. Under this heat flux condition, the maximum temperature in tungsten is predicted to be approximately 2220°C.

Further tests, not reported here for the sake of brevity, have been carried out to assess how the results would change if PFUs with a height of 25 mm (and not 28 mm as in the reference case, so decreasing the thickness of tungsten in the plasma-facing region of 3 mm) are considered. In this case, the maximum temperature value predicted in tungsten is approximately 830°C considering an incident heat flux of 10 MW/m^2, with a 6% deviation with respect to the results reported in [38] for the same geometry.

It can also be seen from the results that the design operating point is on the outer edge of the region in which the circuit can operate. The two constraints delimiting this region are the CHF margin at the IVT and the maximum coolant velocity in the OVT PFU cooling channels. All other constraints are less relevant, including the temperatures in the PFUs. Finally, it can be seen that it is only possible to slightly increase the coolant inlet temperature and its mass flow rate remaining in the acceptable operating region. To increase these parameters, an increase in the coolant inlet pressure is necessary.

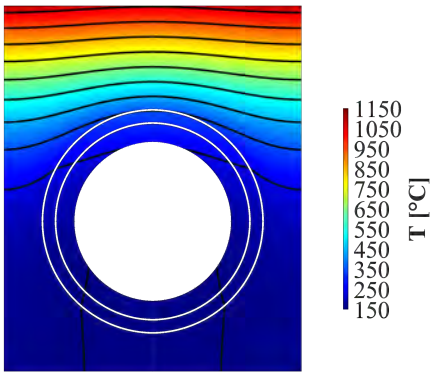

Figure 14: Temperature distributions for an OVT PFU under an incident heat flux of 10 MW/m^2.

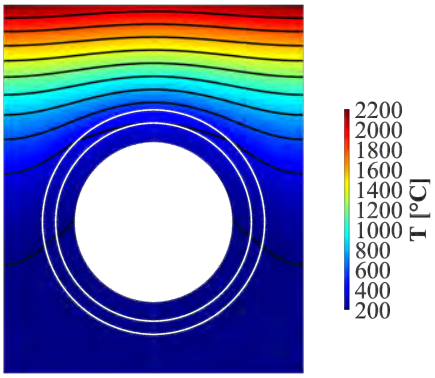

Figure 15: Temperature distributions for an OVT PFU under an incident heat flux of 20 MW/m^2.

6. Application of ADRANOS to the EU-DEMO divertor SCC option cooling circuit

In this section, ADRANOS is employed to study the performance map of the DEMO divertor SCC option, considering the baseline cooling circuit layout and three additional scenarios, in order to explore if it is possible to increase the coolant inlet temperature, in order to improve the component lifetime, according to what discussed in section 3.

6.1. Baseline cooling circuit

The parametric study of the DEMO divertor SCC option has been carried out starting from the cooling circuit layout shown in fig. 8, referring to the results reported in [39] for the hydraulic characterisation. Since CFD results are not available at different values of coolant mass flow rate, it was decided to use an exponent γ for the characteristic function equal to 2. Regarding thermal loads, the surface deposited power of table 1 have been adopted, while volumetric loads obtained from dedicated neutronic analyses of the 2021 divertor design [40] have been considered, whose breakdown is reported in table 6.

Table 6: Deposited volumetric power breakdown for each SCC option divertor cassette.

Component	Power [MW]
CB	0.717
SL	1.558
RPs	0.150
NSs	0.030
IVT	0.620
OVT	0.633
TOTAL	**3.707**

The analysis has been performed considering the coolant inlet pressure at 50, 75, 100, and 150 bar, varying the overall flow rate from 20 to 60 kg/s and the inlet temperature from 70 to 180°C. The selected inlet temperature and mass flow rate ranges have been discretized with 30 points each, for a total of 3600 cases, while the overall run time to perform all the simulations was of approximately 1 hour and 18 minutes on a 3.00 GHz 18 core i9-9980XE workstation.

The results obtained are shown in fig. 16, with reference to the constraints listed in table 4. As it may be argued from the figures, up to about 100 bar of coolant inlet pressure, the operating range of the cooling circuit is limited solely by the pressure drop and the CHF margin of the OVT. Unlike the DCC PFCs cooling circuit previously described, the OVT is the critical component as the two targets are connected in series and the same mass flow rate is distributed across a greater number of PFUs within the OVT, resulting in lower velocities (and thus lower heat transfer coefficients). At even higher pressures, however, the constraint on maximum CuCrZr temperature for the OVT at 10 MW/m^2 comes into play, which is more stringent than the CHF margin, ultimately limiting the maximum coolant inlet temperature to around 154°C.

It should be moreover noted that these results are only qualitative, as such a significant increase in coolant inlet pressure would certainly require a thorough overhaul of the entire EU-DEMO divertor, thus reducing the reliability of the maps presented here. As it may be argued from the results, if the SCC divertor option is chosen to work at lower pressures, i.e. 50 and 75 bar (possibly with no or minor changes in the component de-

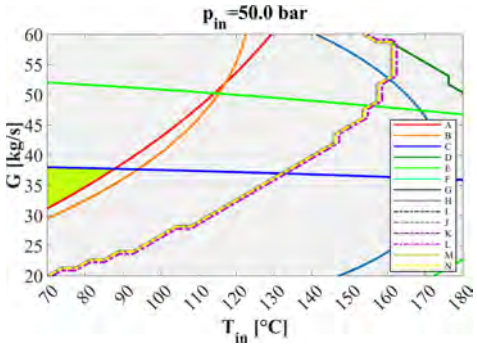

(a)

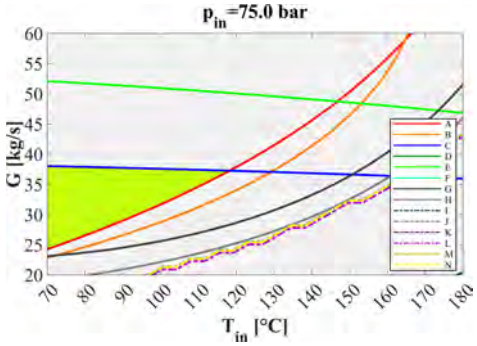

(b)

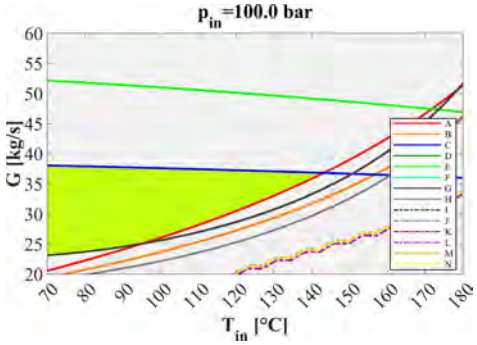

(c)

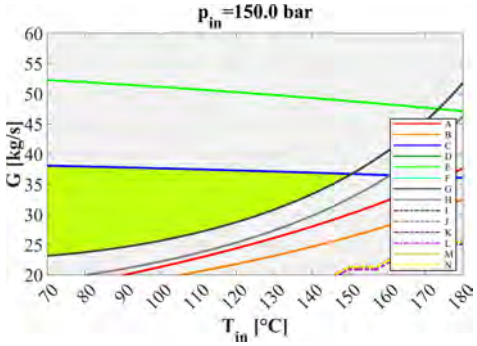

(d)

Figure 16: Range of acceptable operating conditions for the SCC option divertor (in green) for an inlet pressure of 50 (a), 75 (b), 100 (c), and 150 (d) bar.

sign), it would be possible to operate with maximum inlet coolant temperatures of 85 and 115°C, respectively. Using the same reasoning on the maximum irradiation dose damage as in [16], it is therefore possible to estimate the component lifetime of ≈0.8 and ≈0.9 fpy, respectively, which would clearly lead to an unduly reduction of the plant availability.

6.2. Optimized baseline cooling circuit

The first additional scenario foresees an optimisation of the cooling circuit to drastically reduce the total pressure drop. This scenario is highly unlikely, as most of the pressure losses occur in the components directly exposed to the plasma (VTs, SL and RPs), which require high coolant velocities and small tube and channel sizes (thus resulting in high pressure drop) to handle the surface and volumetric loads to which they are subjected. According to this scenario, the maximum coolant operating temperature can certainly be increased, but only to a small extent. In fact, looking at fig. 16a and fig. 16b, it can be seen how, in the absence of the pressure drop constraint, the acceptable operating region of the circuit would be delimited by the OVT CHF margin curve and the maximum velocity in the IVT PFU channels (curve E). Consequently, at an inlet pressure of 50 bar, it would be possible to reach up to ≈115°C coolant inlet temperature, and up to ≈145°C at 75 bar. More realistically, an optimisation of the hydraulic circuit could allow an increase in operating temperature of only a few degrees, not solving the issues related to the component lifetime.

6.3. VTs in parallel

The second scenario relies on the adoption of a parallel connection between the two VTs, as in the case of the PFCs cooling circuit of the DCC option. The flowchart adopted as reference is shown in fig. 17, while loads, characteristic curves and assumptions are the same as those used for the calculation with VTs in series.

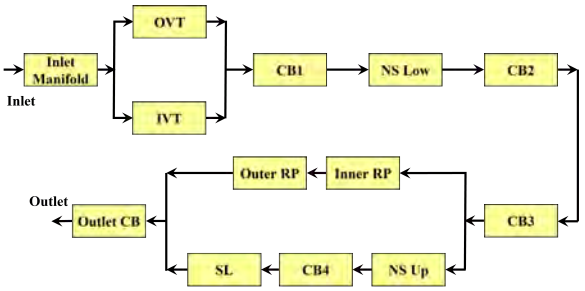

Figure 17: Flowchart of the EU-DEMO divertor SCC option with VTs in parallel.

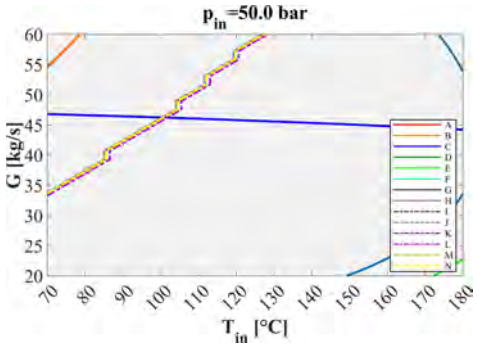

(a)

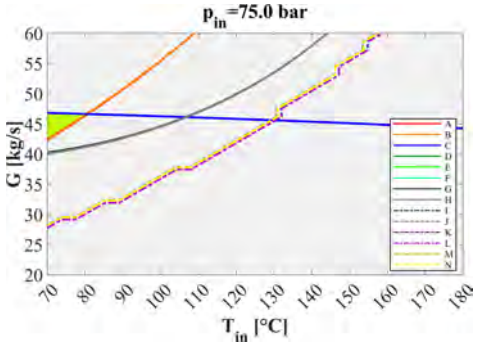

(b)

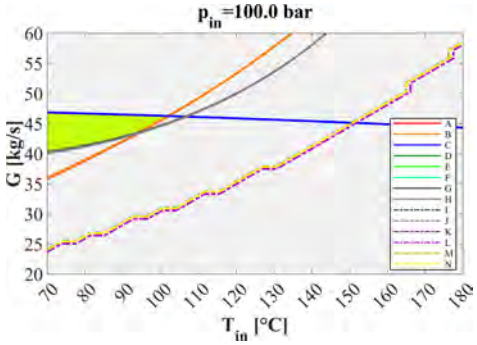

(c)

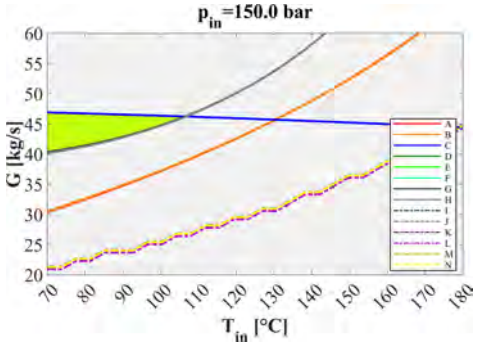

(d)

Figure 18: Range of acceptable operating conditions for the SCC option divertor with VTs in parallel (in green) for an inlet pressure of 50 (a), 75 (b), 100 (c), and 150 (d) bar.

The results obtained are depicted in fig. 18. Considering an inlet coolant pressure of 50 bar, no acceptable operating condition can be found for the circuit, while at higher coolant inlet pressure values, the SCC option with VTs in parallel allows operation only at lower coolant temperatures with respect to the configuration with targets in series. Additionally, by increasing the inlet pressure of the coolant up to 150 bar, it is possible to increase the inlet temperature up to a maximum of about 115°C, beyond which the constraint of the maximum temperature in the CuCrZr comes into play.

6.4. VTs in parallel and CB bypass

Finally, the last scenario analysed involves the presence of a bypass line which ensures that only part of the coolant mass flow rate is fed to the CB, while maintaining the full flow rate at the VTs, in order to prevent the CHF limit curves from moving further to the left (with reference to the previous maps), reducing the region in which the cooling circuit can operate. In the case of series-connected VTs, this is equivalent to a relaxation of the maximum pressure drop constraint, so the results obtained are similar to those of the first additional scenario, i.e. the cooling circuit optimization. In the case of targets in parallel, on the other hand, reference is made to the flowchart shown in fig. 19, where the bypass line is shown in red.

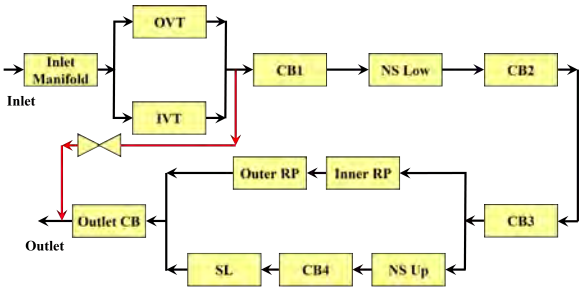

Figure 19: Flowchart of the EU-DEMO divertor SCC cooling option with VTs in parallel and CB bypass.

The bypass line has been modelled by imposing a fixed mass flow rate through the CB equal to 35 kg/s for all the operating conditions of the map, a value close to the one adopted for the DCC option divertor CB [41], so to provide adequate cooling to the components.

In addition, the value of the characteristic curve of the Inlet Manifold component, with reference to fig. 19, has been reduced by a factor of 10, in order to avoid the pressure drops at the inlet could significantly influence the results, being this component designed to route a significantly lower mass flow rate.

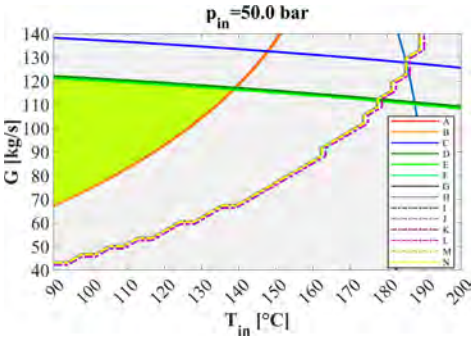

(a)

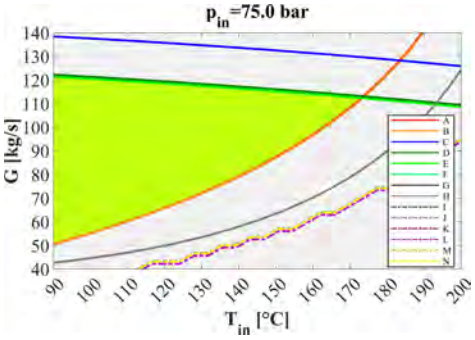

(b)

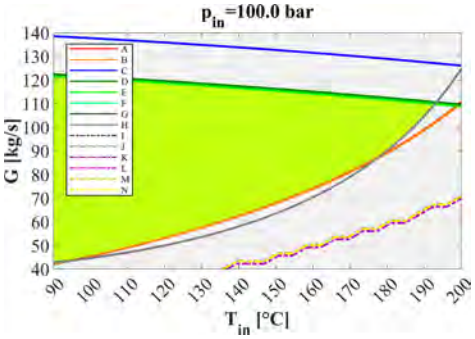

(c)

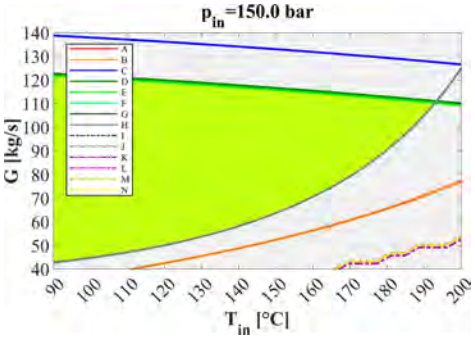

(d)

Figure 20: Range of acceptable operating conditions for the SCC option divertor with VTs in parallel and CB bypass (in green) for an inlet pressure of 50 (a), 75 (b), 100 (c), and 150 (d) bar.

The results obtained are reported in fig. 20. As can be seen, comparing the results shown here with those of the previous sections, the gain obtained with the CB bypass is remarkable, with a maximum value of coolant inlet temperature of about 135°C at 50 bar, 175°C at 75 bar, and 195°C at higher coolant inlet pressure values due to CuCrZr temperature constraints. Although this configuration appears promising, some additional issues should be considered: it is necessary to adopt properly sized orifices downstream of the targets, capable of producing a localized pressure loss of ≈7 bar, resulting in high localized coolant velocities that could cause erosion problems. Moreover, considering the coolant operating point at the maximum allowable coolant inlet temperature of fig. 20d, the orifice alone would result in a loss of fluid mechanical power in the order of ≈60 kW per cassette (approximately equal to the 50% of the pumping power required by both the CB and PFCs cooling circuit of the DCC option [2]), which would have to be supplied to the fluid by the circulation pumps. Finally, it should be further investigated the behaviour of the cooling circuit under transient conditions, and the possibility to establish flow distribution instabilities between the CB and the bypass line, which could potentially pose a risk to the structural integrity of the cassette.

6.5. Summary and discussion on EU-DEMO divertor SCC results

The results obtained considering the baseline topology of the DEMO divertor SCC option and the three additional scenarios discussed above are summarised in table 7.

Table 7: Summary of the results obtained for the different DEMO divertor SCC option cooling circuit topologies.

Maximum coolant inlet temperature			
Scenario	p_{in}=50 bar	p_{in}=75 bar	Max
Baseline	≈85°C	≈115°C	≈155°C
SCC optimization	<115°C	<145°C	<175°C
Par. VTs	-	≈80°C	≈115°C
Par. VTs and Bypass	≈135°C	≈175°C	≈195°C

As can be observed, the most promising single-circuit divertor cooling circuit arrangement is the one with targets in parallel and CB bypass. By adopting this configuration, the coolant inlet temperature, and thus the lifetime of the divertor cassette, can be comparable with the one of the baseline DCC option and, as discussed in section 3, it won't meet the target lifetime requirement. Moreover, also accepting this result, this cooling circuit layout would entail the criticalities discussed in the pre-

vious section, making it doubtful whether this solution may be adopted.

With other cooling circuit layouts and adopting coolant inlet pressure values up to 75 bar, it is realistically not possible to exceed a maximum coolant inlet temperature of ≈120°C, regardless of the VTs arrangement, definitely resulting in a cassette lifetime lower than 1 fpy. At higher pressures, it is possible to increase these values, but, as can be argued from the summary, it is not feasible to obtain the same inlet temperature of the CB circuit as in the DCC configuration, which would lead to a divertor lifetime lower than 1.2 fpy. Furthermore, it would be necessary to significantly change the divertor design in order to withstand the mechanical loads deriving from the increased coolant pressure.

7. Conclusions

In the framework of the activities of the EUROfusion action, UNIPA carried out a research campaign to study the new EU-DEMO divertor SCC option, which foresees the integration of the PFCs and the CB cooling circuits.

In order to evaluate the feasibility in terms of thermal and thermofluid-dynamic performance of this new divertor concept, and to find possible operating conditions able to fulfil the different constraints and requirements of the component, the UNIPA thermo-hydraulic research unit has developed ADRANOS, a coupled lumped-parameter/2D-FEM thermal code. The tool, properly validated, has been used to study the compliance of different layouts of the SCC option with various thermal and thermal-hydraulic constraints, relying on the results of detailed 3D-CFD analyses to obtain data about the characteristic curves of the different subcomponents constituting the divertor.

The analyses highlighted the criticalities of adopting the SCC option for DEMO, as some conflicting constraints must be taken into account, i.e. the CHF margin at the VTs and the overall pressure drop, as well as the need to use a coolant with a sufficiently high temperature to guarantee an acceptable cassette lifetime.

More in detail, the results highlighted how, with the selected cooling circuit configurations, it is possible to find operating conditions compliant with the considered constraints only at relatively low coolant inlet temperature values, thus resulting in a limit on the cassette lifetime, being not possible to meet the target value of 1.5 fpy.

Therefore, although the SCC option divertor would certainly simplify the design of the balance of plant and the cassette maintenance operations, it would require more frequent replacement of the divertor due to the reduction in the component lifetime, thus causing a worsening in terms of nuclear waste, plant availability, and definitely cost. The choice of whether employing the SCC or the DCC option for the EU-DEMO divertor must therefore be made considering the outcomes presented here, which are clearly the result of the actual assumptions in terms of plasma surface heat load, the choice of using Eurofer as structural material for the cassette, the adopted mechanical design rules and the current design and technology of the PFCs, as well as the still incomplete knowledge of the properties of the adopted materials exposed to high levels of neutron-induced damage at low operating temperatures.

CRediT authorship contribution statement

A. Quartararo: Conceptualization, Methodology, Investigation, Writing - original draft. **P.A. Di Maio**: Conceptualization, Methodology, Investigation, Writing - original draft. **E. Vallone**: Conceptualization, Methodology, Investigation, Writing - original draft.

Declaration of Competing Interest

The authors declare that they have no known competing financial interests or personal relationships that could have appeared to influence the work reported in this paper.

Acknowledgments

This work has been carried out within the framework of the EUROfusion Consortium, funded by the European Union via the Euratom Research and Training Programme (Grant Agreement No 101052200 — EUROfusion). Views and opinions expressed are however those of the author(s) only and do not necessarily reflect those of the European Union or the European Commission. Neither the European Union nor the European Commission can be held responsible for them.

References

[1] T. Donné, W. Morris, European Research Roadmap to the Realisation of Fusion Energy, 2018, ISBN: 978-3-00-061152-0.

[2] J. You, et al., Divertor of the european demo: Engineering and technologies for power exhaust, Fusion Engineering and Design 175 (2022) 113010. doi:https://doi.org/10.1016/j.fusengdes.2022.113010.

[3] G. Federici, W. Biel, M. Gilbert, R. Kemp, N. Taylor, R. Wenninger, European DEMO design strategy and consequences for materials, Nuclear Fusion 57 (9) (2017) 092002. doi:10.1088/1741-4326/57/9/092002.

[4] U. Bonavolontà, et al., EU-DEMO divertor: Cassette design and PFCs integration at pre-conceptual stage, Fusion Engineering and Design 159 (2020). doi:10.1016/j.fusengdes.2020.111784.

[5] G. Federici, et al., Overview of the DEMO staged design approach in europe, Nuclear Fusion 59 (6) (2019) 066013. doi:10.1088/1741-4326/ab1178.

[6] A. Quartararo, et al., Thermofluid-dynamic assessment of the EU-DEMO divertor single-circuit cooling option, Fusion Engineering and Design 188 (2023) 113408. doi:https://doi.org/10.1016/j.fusengdes.2022.113408.

[7] J.H.You, et al., Conceptual design studies for the European DEMO divertor: Rationale and first results, Fusion Engineering and Design 109–111 (2016) 1598–1603. doi:10.1016/j.fusengdes.2015.11.012.

[8] P. Di Maio, et al., Hydraulic assessment of an upgraded pipework arrangement for the DEMO divertor plasma facing components cooling circuit, Fusion Engineering and Design 168 (2021) 112368. doi:https://doi.org/10.1016/j.fusengdes.2021.112368.

[9] G. Mazzone, et al., Eurofusion-DEMO Divertor - Cassette Design and Integration, Fusion Engineering and Design 157 (2020) 111656. doi:10.1016/j.fusengdes.2020.111656.

[10] D. Marzullo, et al., DIV-JUS-2-CD1 Divertor System Detailed Design Description, 2020, EUROfusion IDM Ref.: 2NSLJP.

[11] P. Di Maio, G. Mazzone, A. Quartararo, E. Vallone, J. You, Thermal-hydraulic study of the DEMO divertor cassette body cooling circuit equipped with a liner and two reflector plates, Fusion Engineering and Design 167 (2021) 112227. doi:https://doi.org/10.1016/j.fusengdes.2021.112227.

[12] D. Marzullo, et al., DEMO_DIVERTOR_2021_single_cooling, 2022, EUROfusion IDM Ref.: 2PRJTE.

[13] P. Di Maio, et al., On the numerical assessment of the thermal-hydraulic operating map of the DEMO Divertor Plasma Facing Components cooling circuit, Fusion Engineering and Design 161 (2020) 111919. doi:https://doi.org/10.1016/j.fusengdes.2020.111919.

[14] F. Maviglia, et al., Impact of plasma-wall interaction and exhaust on the EU-DEMO design, Nuclear Materials and Energy 26 (2021) 100897. doi:https://doi.org/10.1016/j.nme.2020.100897.

[15] F. Domptail, T. Barrett, M. Fursdon, A. Lukenskas, J.-H. You, The design and optimisation of a monoblock divertor target for DEMO using thermal break interlayer, Fusion Engineering and Design 154 (2020) 111497. doi:https://doi.org/10.1016/j.fusengdes.2020.111497.

[16] G. Mazzone, et al., Choice of a low operating temperature for the DEMO EUROFER97 divertor cassette, Fusion Engineering and Design 124 (2017) 655–658. doi:https://doi.org/10.1016/j.fusengdes.2017.02.013.

[17] The MathWorks, Inc., MATLAB Primer, 2021, Release: R2021b.

[18] FEATool Multiphysics v1.15, User's Guide, 2021. URL https://www.featool.com

[19] A. Raffray, G. Federici, RACLETTE: a model for evaluating the thermal response of plasma facing components to slow high power plasma transients. Part I: Theory and description of model capabilities, Journal of Nuclear Materials 244 (2) (1997) 85–100. doi:https://doi.org/10.1016/S0022-3115(96)00680-0.

[20] T. D. Marshall, D. L. Youchison, L. C. Cadwallader, Modeling the Nukiyama Curve for Water-Cooled Fusion Divertor Channels, Fusion Technology 39 (2P2) (2001) 849–855. doi:10.13182/FST01-A11963345.

[21] Z. Jackson, J. Nicholas, P. Ireland, Development of a 1D thermofluid code for divertor target plate modeling, Fusion Engineering and Design 147 (2019) 111237. doi:https://doi.org/10.1016/j.fusengdes.2019.06.010.

[22] S. E.-D. El-Morshedy, Thermal-hydraulic modelling and analysis of ITER tungsten divertor monoblock, Nuclear Materials and Energy 28 (2021) 101035. doi:https://doi.org/10.1016/j.nme.2021.101035.

[23] M. Holmgren, X Steam, Thermodynamic properties of water and steam, MATLAB Central File Exchange. Retrieved March, 2022 (2022).

[24] International Association for the Properties of Water and Steam, Revised Release on the IAPWS Industrial Formulation 1997 for the Thermodynamic Properties of Water and Steam, 2007.

[25] J. Kiefer, Sequential minimax search for a maximum, Proceedings of the American Mathematical Society 4 (3) (1953) 502–506.

[26] A.R. Raffray, et al., Critical heat flux analysis and R&D for the design of the ITER divertor, Fusion Engineering and Design 45 (4) (1999) 377–407. doi:10.1016/S0920-3796(99)00053-8.

[27] L. Eça, M. Hoekstra, A procedure for the estimation of the numerical uncertainty of cfd calculations based on grid refinement studies, Journal of Computational Physics 262 (2014) 104–130. doi:https://doi.org/10.1016/j.jcp.2014.01.006.

[28] E. Gaganidze, et al., DEMO-DEF-1-CD1 - Materials Properties Handbook - Tungsten, 2020, EUROfusion IDM Ref.: 2P3SPL.

[29] E. Gaganidze, et al., DEMO-DEF-1-CD1 - Materials Properties Handbook - CuCrZr, 2020, EUROfusion IDM Ref.: 2NV3Q6.

[30] Y. S. Touloukian, R. Powell, C. Ho, P. Klemens, Thermophysical Properties of Matter - The TPRC Data Series. Volume 1. Thermal Conductivity - Metallic Elements and Alloys, Tech. rep., Thermophysical and Electronic Properties Information Analysis Center Lafayette, IN (1970).

[31] T. Bergman, A. Lavine, F. Incropera, D. DeWitt, Fundamentals of Heat and Mass Transfer, 8th Edition, Wiley, 2017.

[32] W. Gambill, Heat transfer, burnout, and pressure drop for water in swirl flow through tubes with internal twisted tapes, Vol. 2911, Oak Ridge National Laboratory, 1960.

[33] S. N. Laboratories, U. S. D. of Energy. Office of Scientific, T. Information, FILM-30: A Heat Transfer Properties Code for Water Coolant, United States. Department of Energy, 2001.

[34] A. E. Bergles, W. M. Rohsenow, The Determination of Forced-Convection Surface-Boiling Heat Transfer, Journal of Heat Transfer 86 (3) (1964) 365–372. doi:10.1115/1.3688697.

[35] T. D. Marshall, J. M. McDonald, L. C. Cadwallader, D. Steiner, An Experimental Examination of the Loss-of-Flow Accident Phenomenon for Prototypical ITER Divertor Channels of Y = 0 and Y = 2, Fusion Technology 37 (1) (2000) 38–53. doi:10.13182/FST00-A120.

[36] T. D. Marshall, Experimental examination of the postcritical heat flux and loss-of-flow accident phenomena for prototypical ITER divertor channels, Rensselaer Polytechnic Institute, 1999.

[37] S. E.-D. El-Morshedy, A. Hassanein, Transient thermal hydraulic modeling and analysis of ITER divertor plate system, Fusion Engineering and Design 84 (12) (2009) 2158–2166. doi:https://doi.org/10.1016/j.fusengdes.2009.02.051.

[38] F. Crescenzi, H. Greuner, S. Roccella, E. Visca, J. You, ITER-like divertor target for DEMO: Design study and fabrication test, Fusion Engineering and Design 124 (2017) 432–436. doi:https://doi.org/10.1016/j.fusengdes.2017.02.014.

[39] P. Di Maio, et al., Divertor Thermo-hydraulic assessment 2021, Deliverable DIV-DEMO.S.1-T002-D001, 2022, EUROfusion IDM Ref.: 2PHWSW.
[40] R. Villari, et al., DIV-DEMO.S.1-T003-D001-Neutronics Villari, 2021, EUROfusion IDM Ref.: 2NKBSA.
[41] P. Di Maio, et al., On the thermal-hydraulic performances of the DEMO divertor cassette body cooling circuit equipped with a liner, Fusion Engineering and Design 156 (2020) 111613. doi:https://doi.org/10.1016/j.fusengdes.2020.111613.